Clinical Oral Investigations
https://doi.org/10.1007/s00784-017-2281-1

ORIGINAL ARTICLE

Sugar-based collagen membrane cross-linking increases barrier capacity of membranes

Po-ju Chia-Lai[1] · Anna Orlowska[1] · Sarah Al-Maawi[1] · Andre Dias[1] · Yunxin Zhang[1] · Xuejiu Wang[1,2] · Niklas Zender[1] · Robert Sader[1] · C. James Kirkpatrick[1] · Shahram Ghanaati[1]

Received: 14 March 2017 / Accepted: 20 November 2017

Abstract

Objectives This study examines the permeability and barrier capacity of a sugar cross-linked resorbable collagen membrane ex vivo and in vivo.

Materials and methods In an ex vivo study, injectable platelet-rich fibrin (i-PRF), a peripheral blood-derived human leukocyte-and-platelet-rich plasma was used to analyze membrane permeability. in vivo subcutaneous implantation in Wistar rats ($n = 4$ per time point and group) was used to investigate the barrier capacity of the membrane. The induced in vivo cellular reaction was evaluated at 3, 15, and 30 days and compared to sham OP (control) without biomaterial using histological, immunohistochemical, and histomorphometric methods.

Results Ex vivo, the membrane was impenetrable to leukocytes, platelets, and fibrin from peripheral human blood concentrate (PRF). In vivo, the membrane maintained its structure and remained impervious to cells, connective tissue, and vessels over 30 days. CD-68-positive cell (macrophage) numbers significantly decreased from 3 to 15 days, while from day 15 onwards, the number of multinucleated giant cells (MNGCs) increased significantly. Correspondingly, a rise in implantation bed vascularization from 15 to 30 days was observed. However, no signs of degradation or material breakdown were observed at any time point.

Conclusion Ex vivo and in vivo results showed material impermeability to cellular infiltration of human and murine cells, which highlights the membrane capacity to serve as a barrier over 30 days. However, whether the induced MNGCs will lead to material degradation or encapsulation over the long term requires further investigation.

Clinical relevance The data presented are of great clinical interest, as they contribute to the ongoing discussion concerning to what extent an implanted material should be integrated versus serving only as a barrier membrane.

Keywords Collagen · Guided bone regeneration · Guided tissue regeneration · Foreign body giant cell reaction · Multinucleated giant cells · Barrier membrane

Introduction

Guided bone regeneration (GBR) is a widely used procedure in different surgical fields, especially in oral and maxillofacial surgery [1]. The principle aim is to substitute and support impaired regions due to diseases or traumatic events and to enhance the amount of bone available, such as prior to implant therapy in oral surgery. Since the rate of bone formation is slower than the rate of fibrogenesis, the role of the membrane is first and foremost to prevent the ingrowth of epithelium and connective tissue into the augmentation region [2–4]. Further requirements are to act as a place holder, to maintain space for delayed osteogenesis, and to stabilize the wound in order to achieve primary wound closure [5].

Currently, two types of membranes are commercially available: resorbable and non-resorbable membranes. In the 1990s, non-resorbable membranes, such as expanded polytetrafluoroethylene (e-PTFE), titanium mesh, and titanium-reinforced PTFE, were used in the GBR technique. Although these barriers proved very effective in preventing the invasion of soft tissue physically [6, 7], their technique sensitivity and increased patient

✉ Shahram Ghanaati
shahram.ghanaati@kgu.de

[1] Department for Oral, Cranio-Maxillofacial and Facial Plastic Surgery, FORM (Frankfurt Orofacial Regenerative Medicine) Lab, University Hospital Frankfurt Goethe University, Theodor-Stern-Kai 7, 60590 Frankfurt am Main, Germany

[2] Department of Oral and Maxillofacial Plastic and Trauma surgery, Capital Medical University School of Stomatology, Beijing, China

Published online: 06 December 2017

morbidity (due to obligatory membrane retrieval) were major limitations. To avoid these drawbacks, biomaterials development has been focused on generating resorbable membranes. Among these, collagen, as a ubiquitous molecule, has shown suitable and beneficial properties. Consequently, collagen-based biomaterials have demonstrated favorable GBR results [8] while bypassing the shortcomings of non-resorbable membranes. However, collagen membranes are predisposed to degradation within their implantation beds [9], which undermines their ability to function as true barriers.

During wound healing, different inflammatory cells are involved in the regeneration process of the affected tissue as a cellular response to the injury. In the early wound healing stage and during hemostasis, platelet accumulation occurs to build a platelet plug, which then becomes a fibrin matrix [10]. This phase is then followed by the recruitment of different physiologic mononuclear cells, such as leukocytes and their subtypes, which allows phagocytosis of contaminated and necrotic tissue, first by neutrophils and then by macrophages [10, 11]. Additionally, platelets and leukocytes release numerous growth factors to mediate vascularization [12] and allow the shift to the process of new tissue formation by recruiting keratinocytes and fibroblasts [10].

However, the implantation of biomaterials within the defect area adds an additional factor in the processes of wound healing and tissue regeneration. After biomaterial implantation, an interaction with the biomaterial occurs that results in a biomaterial-specific cellular reaction.

Previously, our group conducted a series of in vivo studies to analyze the cellular reactions towards various collagen membranes of different origins and attributes using a subcutaneous implantation model in small animals. The collected data have shown that, generally, there are two different types of cellular reactions that most likely depend on the physicochemical properties and the processing techniques of the biomaterials. Membranes that induced a physiological reaction by means of mononuclear cells underwent an integration process and maintained their structure over a period of 60 days [7, 13]. This process was revealed in non-cross-linked bilayered collagen membranes of porcine origin composed of collagen types I and III [7], as well as in a collagen-based matrix that included collagen types I and III harvested from porcine peritoneum and skin [13]. Furthermore, the main reaction towards these two collagen-based materials was dominated by mononuclear cells, which ultimately led to its integration within the host tissue without material breakdown [13]. In addition, the cellular reaction in translational clinical cases, including histological evaluation of human samples, corresponded to the in vivo observed outcomes [13].

Other biomaterials demonstrated a different type of cellular reaction that included non-physiological cells, such as multinucleated giant cells (MNGCs), which are a sign of a foreign body reaction [14]. In a comparative in vivo study, two collagen-based biomaterials with different thicknesses were analyzed in a subcutaneous implantation model. Both the thick collagen matrix and the thin bilayered collagen membrane induced the formation of MNGCs, a manifestation of a foreign body reaction [14, 15], which not only led to increased vascularization in the implantation regions but also to membrane breakdown in terms loss of the native structure [14]. Similarly, another in vivo study investigated the cellular responses towards two non-cross-linked collagen-based biomaterials, both of porcine origin but differing in their harvesting compartments and thicknesses, and found that they underwent disintegration by the induction of MNGCs, which led to a breakdown after 30 days in both biomaterials [15]. Therefore, the induced cellular reaction decisively influences the degradation and regeneration process of collagen-based biomaterials and their role as a barrier membrane.

To further increase the resistance of collagen-based biomaterials to degradation, various chemical and physical cross-linking methods, such as ultraviolet light, glutaraldehyde, and enzymatic ribose cross-linking, have been used to boost the biomechanical properties of the collagen fibers [16]. Various studies have shown that supplementary cross-linking confers stability on collagen membranes after implantation [17–19]. However, cross-linking was also associated with foreign body reaction and fibrosis, which might be due to chemical manipulation of the collagen structure [20]. Recently, GLYMATRIX™ technology (Datum Dental Ltd., 1 Bat Sheva Street, Lod 7120101 Israel), a novel technique which uses ribose—a naturally occurring sugar molecule—to cross-link collagen, has been developed [21]. The manufacturing process involves the extraction of collagen into monomeric fibrils, which are then reconstructed and cross-linked to form an improved collagen-based biomaterial. In this study, the capacity of such a sugar cross-linked collagen membrane, OSSIX® PLUS (OS, REGEDENT, Zurich, CH) to serve as a barrier was evaluated in vivo using a subcutaneous implantation model in Wistar rats. Special interest was directed at the induced cellular reaction in terms of cell types, membrane permeability, vascularization, and degradation patterns. Additionally, a blood concentrate system of injectable platelet-rich fibrin (i-PRF), which contains numerous human peripheral blood cells, was used for evaluation of membrane permeability ex vivo.

Materials and methods

OSSIX® PLUS membrane

OSSIX® PLUS membrane (OS) is a sugar cross-linked resorbable collagen membrane derived from porcine tendons [22]. The native tissue undergoes a series of purification

processes to isolate monomeric collagen and to remove all potential immunogenic tissue remnants. Subsequently, the monomeric collagen is reconstituted into collagen fibrils and then glycated with ribose, a naturally occurring sugar, using GLYMATRIX™ technology [21]. Sterilization was achieved with ethylene oxide. The collagen membrane is CE-marked. According to the manufacturer, OS maintains barrier functionality for 4–6 months. Furthermore, since it is purported to be resistant to the oral environment, membrane exposure during implantation will not impede wound healing or guided bone regeneration (GBR) [22]. The biomaterial is specified to be impermeable to cells, but permits the passage of fluid and plasma proteins.

2.2 The study was designed in two separate parts, including ex vivo evaluation and in vivo evaluation:

Experimental design of the ex vivo study part

Injectable platelet-rich fibrin Platelet-rich fibrin (PRF) is a blood concentrate system obtained by the centrifugation of human peripheral blood [23]. This system exists in a solid [23] and a liquid form [24]. PRF is a fully autologous concentrate system that does not require the addition of any external chemicals or anticoagulants. After blood collection, the tubes are immediately centrifuged using a specific, established centrifugation protocol [25]. In the case of the liquid, injectable PRF (i-PRF), the resultant blood concentrate contains a high number of platelets, leukocytes, and plasma proteins suspended in a soluble fibrinogen matrix [24]. Because i-PRF is not treated with anticoagulants, the physiological coagulation process is not inhibited. Therefore, i-PRF forms a clot of cell-loaded fibrin after 10–15 min.

I-PRF preparation and application In the ex vivo section of this study, three healthy volunteers between 18 and 60 years of age, and who were not under any anticoagulant therapy, donated peripheral blood for research purposes. All three volunteers gave written informed consent beforehand. From each participant, venous blood was collected in four 10-ml sterile plastic tubes (Process for PRF, Nice, France). The tubes were immediately centrifuged in a pre-programmed centrifuge (Duo centrifuge, Process for PRF, Nice, France) according to the i-PRF centrifugation protocol (10 ml, 700 rpm, 60 ×*g*, for 3 min) [25]. After this centrifugation process, a multiphasic liquid consisting of a yellowish-orange upper phase and a reddish lower phase was obtained. The former is i-PRF, whereas the latter includes the remaining blood constituents. Using a blunt needle, 1–2 ml of the i-PRF liquid was collected into a 5-ml syringe (Injekt®, B. Braun Medical Inc., Bethlehem, PA, USA) for further use. In the process, care was taken to prevent the two phases from mingling or an accidental uptake of the lower phase.

Four 10 × 10-mm samples of OS were first placed inside a 4 × 6 cell culture plate and then covered by 500 μl i-PRF. After 15 min at room temperature, the i-PRF liquid formed fibrin clots on the OS samples. These OS membrane-fibrin clot samples were then fixed in 4% paraformaldehyde for 24 h to allow for subsequent histological analysis. This experiment was performed in triplicate at independent time points.

Experimental design of the in vivo study part

This study was approved by the Committee on the Use of Live Animals in Teaching and Research of the State of Hessen, Germany. A total of 24 Wistar rats were obtained from Charles River Laboratories (Sulzfeld, Germany) and housed in the Laboratory Animal Unit, Institute of Pathology, Goethe University Frankfurt, Germany. The animals were allowed an acclimation period of 1 week, which enabled them to become accustomed to the new laboratory environment before the experiments began. Throughout the entire study period, the animals were fed regularly with mouse pellets (Laboratory Rodent Chow, Altromin, Lage, Germany) and given water ad libitum. Artificial light–dark cycles of 12 h each simulated day and night rhythms.

Based on the study design, the 24 rats were first assigned randomly into two groups. The animals in the first group ($n = 4$ animals/time point) were implanted with OS, whereas the second group ($n = 4$ animals/time point) served as a sham-operated control in order to evaluate the inflammatory pattern during wound healing without biomaterial implantation. The evaluated time points were 3, 15, and 30 days after implantation. The implantation of OS was performed under sterile conditions in accordance with previously established subcutaneous implantation methods as previously described [13]. All animals survived the operational procedure and through the respective evaluation time points without any complications.

Tissue preparation for histology and histochemistry After explanation at the designated time points, tissue samples as well as ex vivo samples were processed by the methods described in previously published studies [26–28]. First, the samples were fixed in 4% neutral buffered formaldehyde for 24 h. These samples were then placed into embedding cassettes (Histosette, VWR, Deutschland) and dehydrated in baths of progressively concentrated ethanol (70–100%) before alcohol clearance with xylene. Finally, the tissue segments were impregnated with molten paraffin wax and embedded into paraffin blocks. After sufficient cooling, the paraffin blocks were cut with a rotatory microtome (Rotationsmikrotom RM2255, Leica, Germany) to produce serial sections of 3-μm thickness. To evaluate the tissue sections under a microscope, they were stained as follows: the first section was stained with Mayer's hematoxylin and eosin (H&E), while the second section was

stained with Azan. The third section was stained with Masson's trichrome stain, and the fourth section underwent tartrate-resistant acid phosphatase (TRAP) staining. The latter stain was specifically used to identify TRAP activity in target cells. The fifth and sixth and seventh sections were stained immunohistochemically with anti-mouse CD-31, CD-68, and vWF respectively, as previously described [13, 15]. In brief, immunohistochemistry was conducted with a Lab VisionTM Autostainer 360-2D (ThermoFisher Scientific, Germany). After deparaffinization, the slides were pretreated with citrate buffer and proteinase K, followed by H2O2 (UltraVisionTM Quanto Detection System, ThermoFisher Scientific, Germany) and avidin and biotin blocking solutions (Avidin/Biotin Blocking Kit, Vector Laboratories, US). The first antibody used was anti-CD-68 (MCA341GA; 1:400; 30 min), anti-CD-31 (orb10314; 1:200; 2 h), or anti-vWF (ab6994; 1:500; 2 h), whereas the second antibody was goat anti-rabbit IgG-B (sc-2040, 1:200, Santa Cruz Biotechnology, USA). Subsequently, the avidin-biotin-peroxidase complex (ABC) (30 min) and the Histostain-Plus IHC Kit including AEC (20 min) were applied (ThermoFisher Scientific, Germany). Counterstaining was performed using Mayer's hematoxylin. CD-31 and vWF highlight murine blood vessels, while CD-68 detects macrophages in the tissue sections. The negative control for the immunohistochemical staining used was the absence of incubation for primary antibody, while the positive control was applied according to the manufacturer's instruction (anti-CD-31, rat lung; Anti-vWF, human tongue; and anti-CD-68, rat lymph node).

Qualitative histological analysis

Systematic histological assessment was performed by means of a Nikon ECLIPSE 80i microscope (Nikon, Tokyo, Japan) equipped with a motorized stage (ProScan III, Prior, Rockland, MA, USA) and NIS Elements software (Nikon, Tokyo, Japan) as described in preceding publications [14]. Qualitative and quantitative histological analysis focused on the cellular reaction and inflammatory pattern towards the implanted biomaterial, vascularization of the implantation bed, signs of fibrosis, encapsulation, and membrane degradation.

Quantitative histological analysis

Membrane thickness

Adopting the same histomorphometry methods as mentioned in earlier studies [27], the peri-implant tissue of each animal was first digitized prior to histomorphometric analysis. Initially, a total scan including 100–130 individual micrographs was taken automatically by the Nikon ECLIPSE 80i microscope. This was made possible by the motorized stage, which moved automatically within coordinates specified in the NIS Elements software. These single images were then compounded to generate a single large total scan at ×100 magnification. The thickness of the OS membrane of each animal at each of the three time points (3, 15, and 30 days) was then measured at up to 15 distinct points along its length. The mean of these measurements was calculated as the absolute membrane thickness in micrometers. The values obtained from the later time points were also compared to that of day 3, assigned to a value of 100%.

Number of multinucleated giant cells and CD-68-positive mononuclear cells

To analyze the material-associated MNGCs histomorphometrically, TRAP- and CD-68-stained slides were first converted to total scan digital images as previously mentioned. The "annotations and measurements" function of the NIS Elements software was used to manually count the numbers of MNGCs and their subpopulations (TRAP-positive and -negative giant cells), as well as CD-68-positive cells, separately. The respective cell numbers were then computed in relation to the implantation area (MNGCs/mm^2; CD-68/mm^2), and statistical comparison of the different time points was performed to determine the tissue response elicited by OS over the course of the study.

Measurements of membrane vascularization

In a similar fashion, after digitizing the peri-implant region in total scans, the prominently stained blood vessels were manually circumscribed with the area tool of the "annotations and measurements" function of the NIS Elements software. For comparison purposes, the vessel density (vessels/mm^2) and the percentage of vascularization were computed from the total number and total area of vessels in the implantation bed, respectively.

Statistical analysis

The results from the abovementioned histomorphometric analysis were presented as the means ± standard deviation and were evaluated for significant differences at the different time points using a one-way analysis of variance (ANOVA) using GraphPad Prism 6.0 software (GraphPad Software Inc., La Jolla, CA, USA). Differences were considered statistically significant if the P values were* < 0.05 and highly significant if the P values were, **< 0.01, and ***< 0.001 and ****<0.0001. The compiled data were plotted with GraphPad Prism 6.0 software to represent the results graphically.

Results

3.1 Ex vivo histological analysis

The OS membrane was easily identified and exhibited a highly dense structure without detectable pores. The interaction with the i-PRF revealed that no leukocytes or platelets from the i-PRF penetrated into the biomaterial. Instead, OS prevented the inflammatory cells from entering the membrane body. Moreover, the extracellular fibrin was not included within the biomaterial, which resulted in the formation of a cell-rich fibrin clot on both surfaces of the membrane (Fig. 1a, b).

3.2 In vivo histological and histomorphometric analysis

All tested animals survived their respective operations, and healing was uneventful. During the entire experiment, no animals were observed to have necrosis or signs of atypical inflammation.

3.2.1 Tissue reaction to the OS membrane

The OS membrane was clearly visible within the murine subcutaneous implantation bed 3 days after implantation (Fig. 2a). It showed a homogeneous structure of densely packed collagen. Both surfaces of this compact membrane were lined with a layer of mononuclear cells (Fig. 2a, b), of which a large amount were CD-68-positive, i.e., macrophages. No penetration by peri-implant cells or extracellular matrix was noted at this time point (Fig. 4a, A1). Thus, the membrane per se was free of cells. Single vessels were found within the peri-implantation area, but the membrane itself exhibited no vascularization (Fig. 3 A).

On day 15 post-implantation, the membrane did not show any signs of degradation (Fig. 2c, d). In comparison to day 3, more mononuclear cells were observed in the implantation bed (Fig. 5b), several of which were CD-68-positive (Fig. 4b, B1). Additionally, a small number of MNGCs located predominantly at the biomaterial-tissue interface was seen (Fig. 2d). A majority of these MNGCs was TRAP-negative (Fig. 5c). At this time point, the membrane maintained its structure, preventing cellular infiltration into the membrane central region. Moreover, connective tissue formation was observed only within the peri-implantation region, and no connective tissue ingrowth was detected within the membrane. Although micro-vessel formation was noted in proximity to the membrane, the membrane body itself remained avascular (Fig. 5a, Fig. 3b). Additionally, no signs of membrane breakdown were observed at this time point.

At day 30 after implantation, no evidence of degradation of the membrane was perceived (Fig. 2e). The membrane displayed a stable dense structure and inhibited cellular infiltration of all kinds. Instead, an organized, cell-rich connective tissue was seen on both membrane surfaces (Fig. 5e). In comparison to day 15, the number of mononuclear cells adjacent to the membrane increased significantly (Fig. 2e, f). These included CD-68-positive cells (Fig. 4c, C1). In addition, more biomaterial-adherent MNGCs were identified within the implantation region (Fig. 2f), which remained on the membrane surface and did not enter the biomaterial body. The majority of the MNGCs showed no TRAP expression. Nevertheless, no signs of membrane

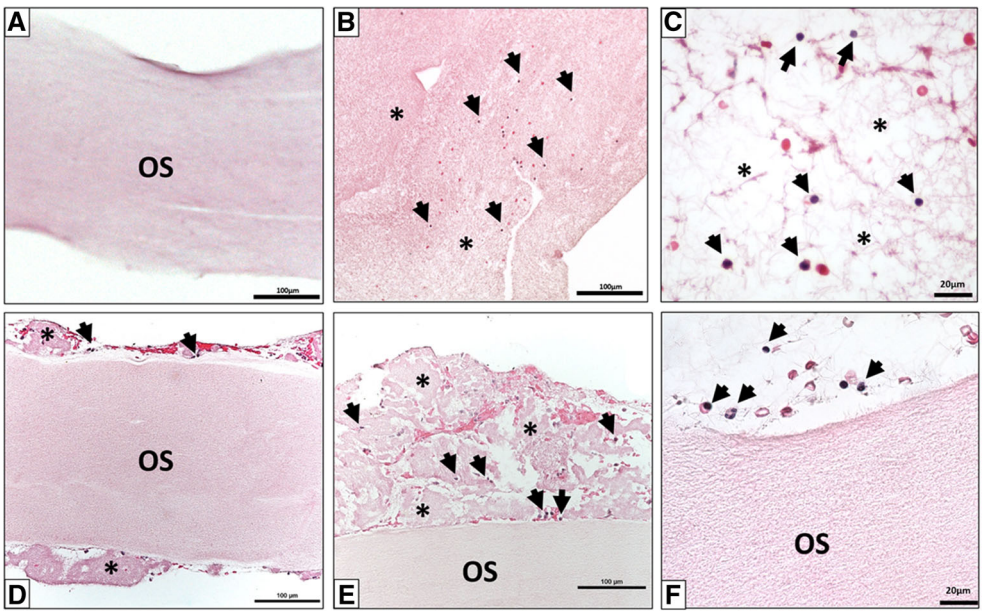

Fig. 1 **a** The native structure of OS membrane ex vivo as a control in H&E staining at ×100 magnification. **b** i-PRF alone in H&E staining at ×200 magnification; asterisk = fibrin clot, black arrows = human leukocytes. **c** i-PRF alone; black arrows = human leukocytes, asterisk = fibrin clot in H&E staining ×600 magnification. **d** A cross section of the OS membrane treated with i-PRF in H&E staining at ×100 magnification. **e** The interface between i-PRF and OS in H&E staining at ×200 magnification; asterisk = fibrin clot, black arrows = human leukocytes. **f** Black arrows = human leukocytes in H&E staining ×600 magnification

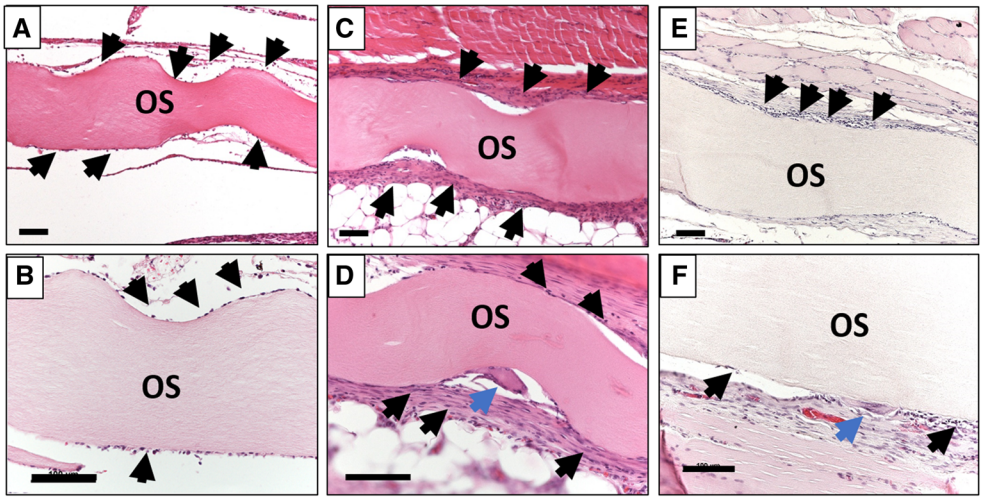

Fig. 2 **a** The membrane (OS) within the implantation bed on day 3. Mononuclear cells were detected on both membrane surfaces (black arrows). **b** Mononuclear cells on the membrane (OS) surface (black arrows) on day 3. **c** The membrane (OS) within the implantation region on day 15. There is an increased number of mononuclear cells on both membrane surfaces (black arrows). **d** Mononuclear cells (black arrows), as well as multinucleated giant cells (blue arrow) on the membrane surface (OS) on day 15. **e** The membrane within the implantation bed (OS) on day 30. **f** Mononuclear (black arrows) and multinucleated giant cells adhering to the membrane (OS) surface on day 30. (H&E staining; **a**, **c**, **e** at ×100 magnification; **b**, **d**, **f** at ×200 magnification; all scale bars = 200 μm)

breakdown were found (Fig. 5f). Although the membrane continued to be impermeable to cells and connective tissue, there were no indications that it was segregated from the surrounding tissue by encapsulation or fibrosis.

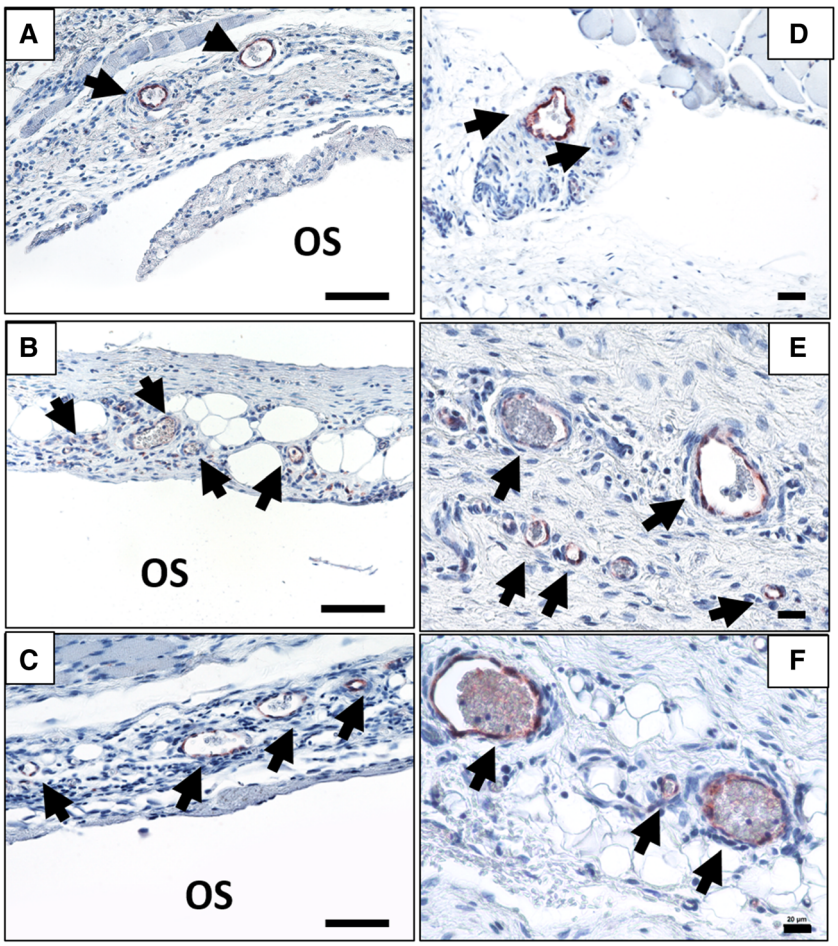

Fig. 3 The vascularization pattern over the investigation time points using immunohistochemical stains: **a**–**c** = anti-CD-31; × 200 magnification; scale bar = 100 μm. **d**–**f** = anti-vWF; ×00 magnification; scale bar = 20 μm. Black arrows indicate vessels and OS indicates the membrane

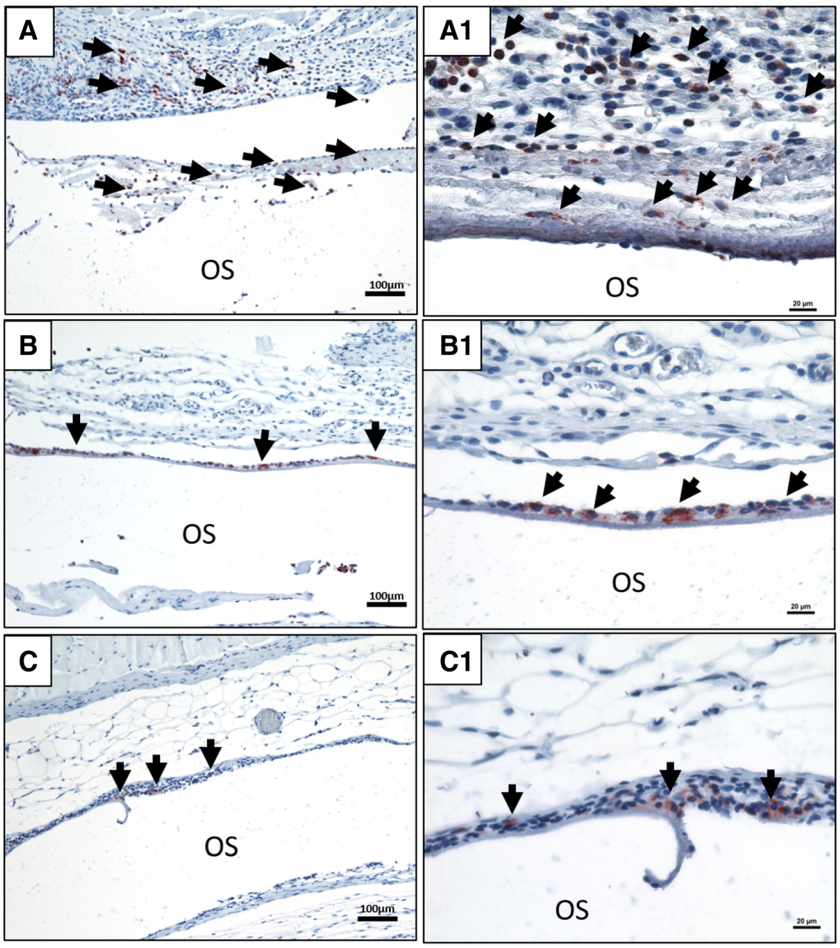

Fig. 4 The CD-68-positive cells on the biomaterial surface at day 3 (**a**; A1); day 15 (**b**; B1) and day 30 (**c**; C1). Black arrows = CD-68-positive mononuclear cells, i.e., macrophages. OS indicates the biomaterial. In **b** and **c**, the biomaterial was detached and washed during the staining process. **a**–**c** × 100 magnification; 100-µm scale bar. A1–C1 ×400 magnification; 20-µm scale bar

3.2.2 Histomorphometric results

Histomorphometric analysis of OS membrane thickness The histomorphometric analysis of the OS membrane revealed that there was no decrease in membrane thickness between day 3 and day 30 after implantation. In contrast, the measured membrane thickness showed a slight increase over the study period, which was not statistically significant (day 3 = 274.68 ± 27.75; day 15 = 287.59 ± 27.83; day 30 = 302.60 ± 15.19), (Fig. 6a). Due to the possibility of artifacts arising from the histological and implantation procedures, the membrane thickness was calculated as a percentage to obtain a more accurate evaluation. The thickness of day 3 was set at 100%, and all mean values of successive time points were calculated in relation to day 3. The percentage of thickness revealed a slight increase of the membrane thickness towards day 30. However, no statistically significant differences were detected over the duration of the study (day 15 = 104.70% ± 15.93%; day 30 = 110.11% ± 15.77%; Fig. 6b).

Histomorphometric analysis of CD-68-positive macrophages At day 3 post-implantation, the macrophage density in the peri-implant area was significantly higher than that of day 15 ($P < 0.1$) and day 30 ($P < 0.1$). There was no statistically significant increase in the density of the macrophages in the implantation bed between day 15 and day 30. A similar trend was observed within the control group, which showed that the number of macrophages decreased significantly from day 3 to 15, (day 3 vs. day 15 ($P < 0.5$); day 3 vs. day 30 ($P < 0.1$)). In contrast, there was no statistically significant difference between days 15 and 30 (data not shown). However, the number of macrophages within the OS group was significantly higher than that of the control group at all time points (day 3 ($P < 0.001$); day 15 ($P < 0.1$); day 30 ($P < 0.001$), Fig. 7b).

Histomorphometric analysis of multinucleated giant cells At day 3 after implantation, no MNGCs could be detected within the area of implantation. Their presence was first observed at day 15 after implantation. The number of MNGCs at day 15 was highly significant compared to day 3 ($P < 0.001$). Moreover, the majority of the MNGCs was TRAP-negative, and the difference between day 3 and day 15 was statistically significant ($P < 0.01$). The membrane-adherent TRAP-positive MNGCs at day 15 showed no statistical significance when compared between day 3 and day 15. However, at day 30, the total number of MNGCs increased significantly

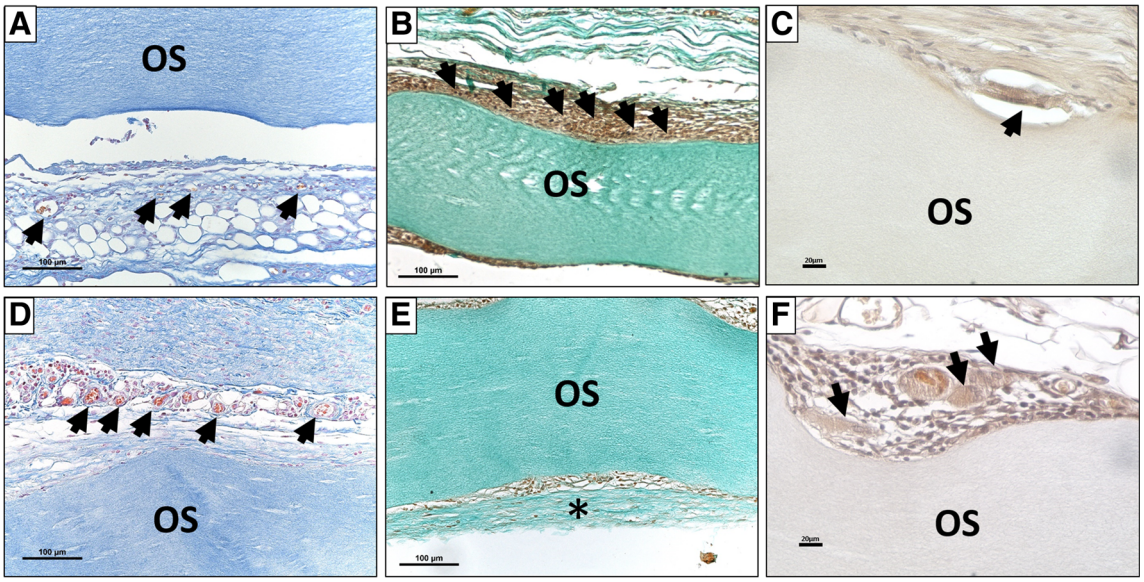

Fig. 5 Detailed representative micrographs on days 15 and 30. **a** Vessels (black arrows) were detected near the membrane (OS) at day 15, (Azan staining; ×200 magnification; scale bar = 100 μm). **b** Accumulation of mononuclear cells (black arrows) on the membrane (OS) surface at day 15, (Masson Goldner staining; ×400 magnification; scale bar = 20 μm). **c** TRAP-negative multinucleated giant cells (black arrows) adherent on the membrane (OS) surface at day 30 (TRAP staining; ×400 magnification; scale bar = 20 μm). **d** Increased numbers of vessels (black arrows) were detected in proximity to the membrane (OS) at day 30, (Azan staining; ×200 magnification; scale bar = 100 μm). **e** Formation of organized connective tissue including mononuclear cells (asterisk) on the membrane (OS) surface at day 30, (Masson Goldner staining; ×400 magnification; scale bar = 20 μm). **f** TRAP-negative multinucleated giant cell (black arrows) adherent on the membrane (OS) surface at day 30 (TRAP staining; ×400 magnification; scale bar = 20 μm)

compared to day 3 ($P < 0.0001$) and day 15 ($P < 0.0001$). Additionally, the number of TRAP-negative MNGCs was significantly higher than at day 3 ($P < 0.0001$) and day 15 ($P < 0.0001$). In contrast, the number of TRAP-positive MNGCs was notably constant, and there was no significant difference between day 3, day 15, and day 30 (Fig. 7a).

The control group showed no multinucleated giant cells at any time point.

Histomorphometric analysis of the implantation bed vascularization Histomorphometric evaluation of the implantation bed showed that no ingrowth of vessels into the membrane was detected at any time points during the study. The percentage of vascularization in the peri-implantation bed increased steadily over the course of the study. At day 3 after implantation, the percentage of vascularization was comparable to that of the control group. At day 15 post-implantation, there was no statistically significant increase in the vascularization percentage compared to day 3. In addition, no statistically significant difference was detected between the test group and the control group. However, at day 30, the percentage of vascularization was significantly higher in comparison to day 3 ($P < 0.0001$) and day 15 ($P < 0.001$), respectively. At this time point, the vascularization percentage in the test group was significantly higher than that in the control group ($P < 0.05$). Similarly, the percentage of vascularization increased gradually in the sham-operated groups as well (Fig. 6c).

The number of vessels detected per square millimeter at day 3 was significantly higher than that of the control group ($P < 0.01$). Comparing the values at day 15 to day 3, no statistically significant difference between the test groups was found. However, at day 15, the value in the test group was significantly higher than that of the control group ($P < 0.01$). Moreover, at day 30 post-implantation, there was a marked increase in the number of vessels per square millimeter. This value was highly statistically significant compared to both day 3 and day 15 ($P < 0.0001$). At this time point, the difference in vessel number per square millimeter was also highly significant compared to the control group ($P<0.0001$) (Fig. 7d).

Discussion

The present study evaluated a collagen membrane reinforced using a ribose cross-linking technique. The aim of the study was to analyze cellular permeability of this biomaterial ex vivo and its barrier capacity in vivo. Special interest was directed to the cellular reaction towards this biomaterial in terms of the induced cell types and vascularization and degradation pattern compared to the control sham operation group, which imitated the physiological wound healing process.

In the ex vivo part, the focus was placed on evaluating the cellular permeability of the biomaterial. Looking at the clinical scenario, after biomaterial application, the membrane first

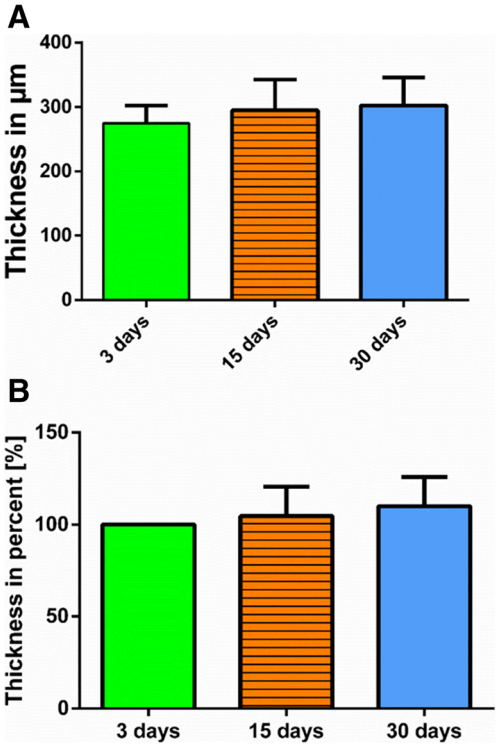

Fig. 6 **a** Illustration of the histomorphometric analysis of the membrane thickness in micrometers. **b** Illustration of the histomorphometric analysis of the membrane thickness as a percentage relative to day 3

comes in contact with the blood. Therefore, injectable platelet-rich fibrin (i-PRF), which is a blood concentrate system derived from centrifuged human peripheral blood, was chosen for this examination. I-PRF can be considered a cell suspension containing cells that are involved in wound healing, such as platelets and leukocytes [29]. In this context, the pattern of interaction with i-PRF might provide several hints concerning the initial cellular interactions with the biomaterial. The results of the ex vivo part showed that OS was occlusive to the cells and fibrin of the i-PRF and prevented cellular penetration into the membrane body. These results underline the impenetrability of OS to soluble plasma and proteins, such as the fluid fibrin.

The in vivo study focused on the barrier capacity of OS over 30 days and the induced cells in comparison to the cells involved in wound healing of the control group. In vivo histological analysis revealed no cellular penetration of the membrane at any time point. In short, both ex vivo human cells and in vivo murine inflammatory cells were not detected within the membrane. This comparison between the ex vivo and in vivo studies is noteworthy, as it was demonstrated in this study that it is possible to determine the barrier capacity and to obtain clues regarding the cellular response of biomaterials by using a human-derived cell-rich blood concentrate, i-PRF, to reach results similar to those obtained by in vivo animal experiments. However, further applications of this method are necessary to evaluate the potential of i-PRF to serve as an alternative to in vivo animal experimentation to assess immediate and early tissue reactions towards biomaterials.

Histological analysis of the cellular reaction showed that the membrane induced an initial mononuclear cell-based reaction at day 3. At this time point, a large number of CD-68-positive cells, macrophages, were detected within the implantation bed. Thus, at the mid-term evaluation time point, day 15, a course change in the inflammatory pattern was observed. During this time, the number of CD-68-positive cells significantly decreased, coincident with the appearance of multinucleated giant cells (MNGCs). The trend of the CD-68 accumulation was similar to the control group wound healing. However, OS induced significantly higher numbers of CD-68 cells at all time points. In addition, no MNGCs were found in the control group at any time point. This significant reduction in the number of CD-68 cells towards days 15 and 30 in the OS group might be related to the physiological presence of macrophages in an increased number during the initial phase of the wound healing and their physiological persistence period within the wounded site, as was the case in the control group [10]. However, the high number of CD-68-positive cells within the OS group in comparison to the control group showed a higher rate of inflammation due to the biomaterial, which might have led to the persistence of a specific type of macrophages that is not only involved in wound healing but also in so-called "frustrated phagocytosis" [30, 31], a process of foreign body giant cell formation in which macrophages fuse to form MNGCs after their efforts to phagocytize the implanted biomaterial proved futile. From day 15 to day 30, the number of CD-68-positive cells showed no significant difference, but the number of MNGCs significantly increased. It might be deduced that newly recruited macrophages progressively fused to form MNGCs as the collagen biomaterial continued to persist in the implantation region. In this context, the observed cellular response also might be partly due to the surface topography of OS, as the surface properties of biomaterials influence the type of proteins that adhere to the biomaterial surfaces [13]. This impacts the adhesion and subsequent polarization of macrophages downstream, the amount and types of cytokines they secrete, and, eventually the fusion of these macrophages into MNGCs [32, 33].

The material-adherent MNGCs were mostly TRAP-negative. Only single TRAP-positive MNGCs were located within the implantation region, and their numbers displayed no statistically significant increase over the study period. The presence of MNGCs within the implantation bed indicated a foreign body reaction towards the evaluated membrane [31], although the role of biomaterial-related MNGCs is still mostly unexplored.

The aforementioned significant increase in the total number of MNGCs between day 3, day 15, and day 30 also contributed to a significant rise in implantation bed vascularization between the analyzed time points. The MNGCs might have

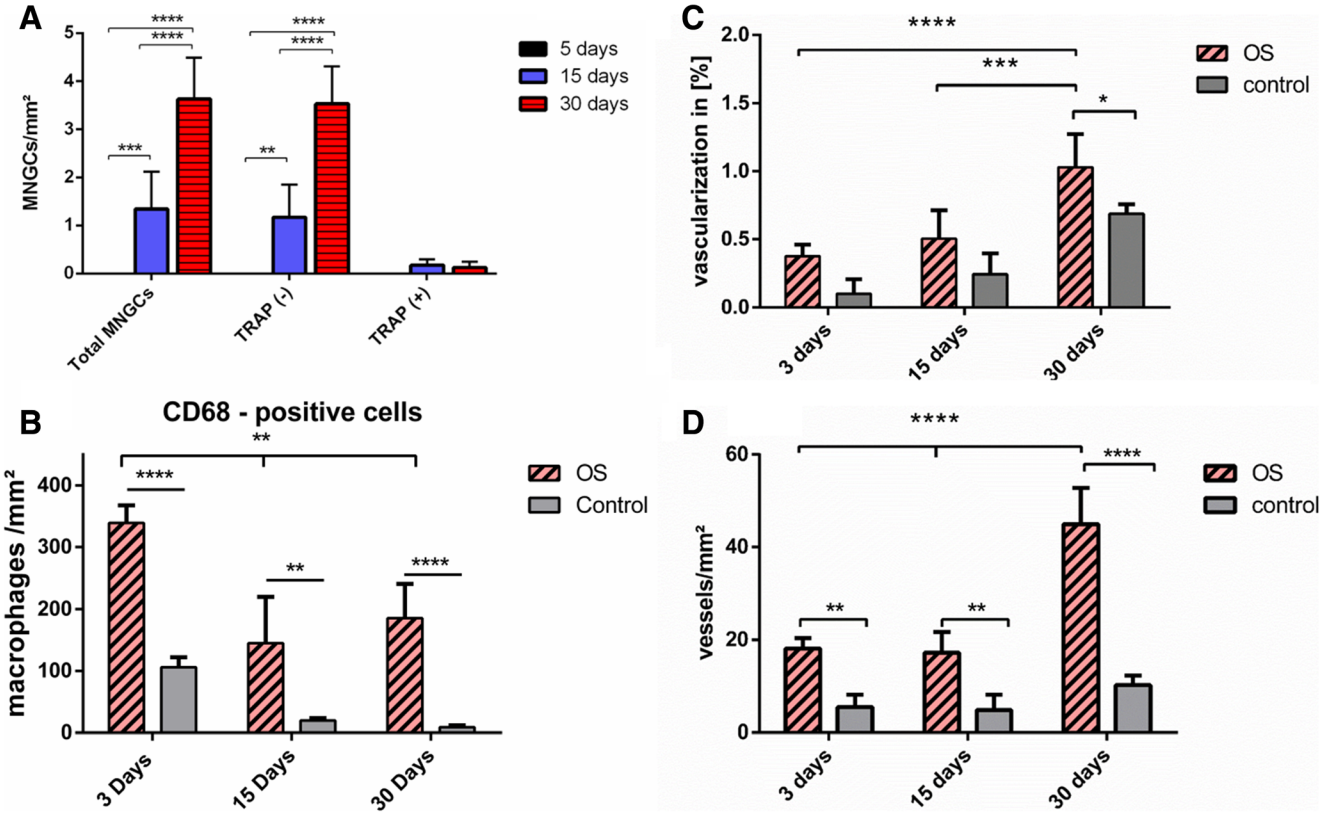

Fig. 7 Comparative graphical presentation of the histomorphometric statistical analysis over the study period. Values are illustrated as means and SD. **a** The number of total multinucleated giant cells (MNGCs) and TRAP-positive and TRAP-negative MGCSs per square millimeter. **b** The total number of macrophages (CD-68-positive cells) per square millimeter. **c** The vascularization rate over the study time in the OS test group and the control group. The vessel area was calculated as a percentage of the total examined area. **d** The number of vessels per square millimeter in the OS test group and the control group. * = $P < 0.05$, ** = $P < 0.1$, *** = $P < 0.01$, and **** = $P < 0.001$

contributed to the increase in implantation bed vascularization, since it is known that MNGCs secrete vascular endothelial growth factor, a main protagonist of neoangiogenesis [12, 34]. These findings verify the present results, which highlight the correlation between the enhanced vascularization and the increase in the number of MNGCs within the implantation bed of collagen-based biomaterials. Taken together, the significant increase in the number of MNGCs and the significant rise in implantation bed vascularization over the course of the study are indicative of a foreign body reaction.

Interestingly, recent studies have shown that the presence of MNGCs within the implantation bed of the non-cross-linked collagen membrane led to its disintegration by premature connective tissue ingrowth and eventual membrane breakdown. In these studies, the correlation between the increased number of MNGCs and the enhanced implantation bed vascularization bears resemblance to our current findings [13, 35]. Although MNGCs boast enhanced oxidative and phagocytic capabilities compared to macrophages alone [36, 37], the significant increase in the vascularization and number of MNGCs in the present study did not alter the integrity of OS over 30 days. In contrast, the membrane remained fully intact, without exhibiting any signs of cellular penetration, degradation, or membrane breakdown over the observation period of 30 days. Moreover, as OS is derived from porcine tendons, it is different from the other membranes investigated earlier by our study group, which are either processed from the porcine dermis and/or pericardium [13–15]. In this context, the quality and the harvesting compartment of the used collagen might play a crucial role in its degradation pattern and therefore its barrier function.

Other studies conducted by our group have shown that several biomaterials induce a full physiological reaction without the formation of MNGCs, such as a non-cross-linked gamma-sterilized collagen membrane that maintained its structure over a period of 60 days. It underwent a slow and controlled integration by inducing a mere mononuclear reaction that was similar to the wound healing physiological reaction that was observed in the control group of the present study. Moreover, these mononuclear cells were accompanied by a mild vascularization. This membrane elicited a physiological mononuclear reaction and mild vascularization pattern. The integration of the membrane was achieved by allowing the host cells to slowly migrate into the membrane scaffold while preserving the function, structure, and the functional barrier of the membrane [13].

Despite the formation of MNGCs, in an in vivo study in a dog model, OS was used to cover critical size defects within the jaw after tooth extraction. After 25 weeks, OS showed signs of ossification and led to enhanced bone regeneration compared to sham OP [38]. The manufacturing technique of OS also makes it highly interesting, as the collagen fibrils are reconstituted de novo from extracted monomeric collagen, whereas conventional membranes are assembled from residual in situ collagen after the removal of all immunogenic components from the donor tissue. Another distinct characteristic of OS is the incorporation of ribose to cross-link the collagen fibrils by a patented glycation process, GLYMATRIX™ [21]. In a way, OS simulates glycation by glucose, a well-documented occurrence in aging tissue and diabetes, which grants collagen fibers resistance to degradation by collagenase [39, 40].

In comparison, other cross-linking methods, such as chemical cross-linking with glutaraldehyde, evoked a more aggressive inflammatory reaction [41]. In addition, clinical human studies have shown that even when exposed to the oral environment, OS sustained GBR and GTR functions compared [18, 42]. Additionally, a case series in which OS was applied for GBR in implant-related bony defects showed that 25–29 weeks after primary healing, new bone formation was observed in close proximity to the OS showing partial signs of ossification [43].

The actual results in OS resemble the cellular reaction observed with e-PTFE, a non-resorbable membrane that displayed a similar inflammatory pattern and cellular reaction to the currently evaluated membrane OS. In brief, e-PTFE elicited an initial mononuclear cell-based reaction, which was followed by the formation of MNGCs. e-PTFE, which served as a bona fide physical barrier, prevented cellular infiltration for an investigation period of 60 days. Accordingly, the e-PTFE membrane was encapsulated within a vessel- and MNGC-rich connective tissue after 60 days [7]. No encapsulation could be detected at the latest time point of this study. Nevertheless, the limited evaluation period of 30 days is likely insufficient to evaluate whether the membrane will ultimately undergo encapsulation. Therefore, further long-term studies are needed to assess to what extent the presence of MNGCs within the implantation bed of this specific cross-linked biomaterial might influence the regeneration process, which is thought to be guided by OS.

Additionally, one limitation of the in vivo part of this study is analyzing only sugar-based without PRF. Thereby, this study cannot make any statement about the in vivo cellular reaction to OS-i-PRF combination. The implantation of i-PRF in small animals would require the use of severe combined immunodeficiency (SCID) mice to avoid any immune reaction to the implanted human cells. Ongoing research is towards understanding the in vivo cellular reaction to PRF and its combination with different biomaterials. This application might be a tool to modulate the cellular reaction towards biomaterials by means of pre-loading with i-PRF in advance.

Conclusion

The present study evaluated, the permeability and barrier capacity of a ribose cross-linked collagen membrane ex vivo as well as in vivo, with specific respect to the induced cell types. Ex vivo, the membrane was impermeable to human cells derived from peripheral blood. In vivo, the membrane showed a stable structure and allowed no cellular penetration over 30 days. The in vivo cellular reaction was initiated by mononuclear cells, which progressed to the formation of multinucleated giant cells (MNGCs) from day 15 onwards. Over the course of the experiment, a significant increase in the number of MNGCs was associated with a significant rise in implantation bed vascularization. This is indicative of a foreign body reaction. However, no breakdown was observed at any time point. The data gathered prove that ribose cross linking enhanced the barrier functionality of the collagen membranes. On these grounds, further long-term studies are necessary to investigate the degradation pattern of this specific cross-linked biomaterial.

Acknowledgments The authors would like to thank Mrs. Verena Hoffmann for her excellent technical assistance. This work was partially funded by Marie Curie Actions under EU FP7 Initial Training Network SNAL 608184.

Funding This research was funded solely by the FORM Lab's own research funds.

Compliance with ethical standards

Conflict of interest The authors declare that they have no conflict of interests.

Ethical approval All applicable international, national, and/or institutional guidelines for the care and use of animals were followed.

Informed consent For the ex vivo part, informed consent was obtained from all individual participants included in the study.

References

1. Bottino MC, Thomas V, Schmidt G, Vohra YK, Chu T-MG, Kowolik MJ, Janowski GM (2012) Recent advances in the development of GTR/GBR membranes for periodontal regeneration—a materials perspective. Dent Mater 28(7):703–721. https://doi.org/10.1016/j.dental.2012.04.022
2. Cen L, Liu W, Cui L, Zhang W, Cao Y (2008) Collagen tissue engineering: development of novel biomaterials and applications. Pediatr Res 63(5):492–496. https://doi.org/10.1203/PDR.0b013e31816c5bc3
3. Dahlin C, Linde A, Gottlow J, Nyman S (1988) Healing of bone defects by guided tissue regeneration. Plast Reconstr Surg 81(5):672–676. https://doi.org/10.1097/00006534-198805000-00004
4. Patino MG, Neiders ME, Andreana S, Noble B, Cohen RE (2002) Collagen as an implantable material in medicine and dentistry. Research 220

5. Wang H-L, Boyapati L (2006) "PASS" principles for predictable bone regeneration. Implant Dent 15:8–17. https://doi.org/10.1097/01.id.0000204762.39826.0f
6. Buser D, Dula K, Hirt HP, Schenk RK (1996) Lateral ridge augmentation using autografts and barrier membranes: a clinical study with 40 partially edentulous patients. J Oral Maxillofac Surg 54: 420–432 3
7. Ghanaati S (2012) Non-cross-linked porcine-based collagen I-III membranes do not require high vascularization rates for their integration within the implantation bed: a paradigm shift. Acta Biomater 8(8):3061–3072. https://doi.org/10.1016/j.actbio.2012.04.041
8. Sheikh Z, Qureshi J, Alshahrani AM, Nassar H, Ikeda Y, Glogauer M, Ganss B (2016) Collagen based barrier membranes for periodontal guided bone regeneration applications. Odontology. https://doi.org/10.1007/s10266-016-0267-0
9. Bunyaratavej P, Wang HL (2001) Collagen membranes: a review. J Periodontol 72(2):215–229. https://doi.org/10.1902/jop.2001.72.2.215
10. Gurtner G, Werner S, Barrandon Y, Longaker M (2008) Wound repair and regeneration. Nature 453(7193):314–321. https://doi.org/10.1038/nature07039
11. Shevach EM, Rosenthal AS (1973) Function of macrophages in antigen recognition by guinea pig T lymphocytes. II. Role of the macrophage in the regulation of genetic control of the immune response. J Exp Med 138:1213–1229 http://www.ncbi.nlm.nih.gov/pubmed/4126770. Accessed 20 March 2017
12. Moens S, Goveia J, Stapor PC, Cantelmo AR, Carmeliet P (2014) The multifaceted activity of VEGF in angiogenesis—implications for therapy responses. Cytokine Growth Factor Rev 25(4):473–482. https://doi.org/10.1016/j.cytogfr.2014.07.009
13. Ghanaati S, Schlee M, Webber MJ, Willershausen I, Barbeck M, Balic E, Görlach C, Stupp SI, Sader RA, Kirkpatrick CJ, Ghanaati S (2011) Evaluation of the tissue reaction to a new bilayered collagen matrix in vivo and its translation to the clinic. Biomed Mater 6(1): 15010–15012. https://doi.org/10.1088/1748-6041/6/1/015010
14. Barbeck M, Lorenz J, Kubesch A, Böhm N, Booms P, Choukroun J, Sader R, Kirkpatrick CJ, Ghanaati S (2015) Porcine dermis-derived collagen membranes induce implantation bed vascularization via multinucleated giant cells: a physiological reaction? J Oral Implantol 41(6):e238–e251. https://doi.org/10.1563/aaid-joi-D-14-00274
15. Barbeck M, Lorenz J, Holthaus MG, Raetscho N, Kubesch A, Booms P, Sader R, Kirkpatrick CJ, Ghanaati S (2015) Porcine dermis and pericardium-based, non-cross-linked materials induce multinucleated giant cells after their in vivo implantation: a physiological reaction? J. Oral Implantol. 41(6):e267–e281. https://doi.org/10.1563/aaid-joi-D-14-00155
16. Brunel G, Piantoni P, Elharar F, Benqué E, Marin P, Zahedi S (1996) Regeneration of rat calvarial defects using a bioabsorbable membrane technique: influence of collagen cross-linking. J Periodontol 67(12):1342–1348. https://doi.org/10.1902/jop.1996.67.12.1342
17. Friedmann A, Strietzel FP, Maretzki B, Pitaru S, Bernimoulin J-P (2002) Histological assessment of augmented jaw bone utilizing a new collagen barrier membrane compared to a standard barrier membrane to protect a granular bone substitute material. Clin Oral Implants Res 13(6):587–594. https://doi.org/10.1034/j.1600-0501.2002.130603.x
18. Moses O, Pitaru S, Artzi Z, Nemcovsky CE (2005) Healing of dehiscence-type defects in implants placed together with different barrier membranes: a comparative clinical study. Clin Oral Implants Res 16(2):210–219. https://doi.org/10.1111/j.1600-0501.2004.01100.x
19. Friedmann A, Gissel K, Soudan M, Kleber B-M, Pitaru S, Dietrich T (2011) Randomized controlled trial on lateral augmentation using two collagen membranes: morphometric results on mineralized tissue compound. J Clin Periodontol 38(7):677–685. https://doi.org/10.1111/j.1600-051X.2011.01738.x
20. Rothamel D, Schwarz F, Sager M, Herten M, Sculean A, Becker J (2005) Biodegradation of differently cross-linked collagen membranes: an experimental study in the rat. Clin Oral Implants Res 16(3):369–378. https://doi.org/10.1111/j.1600-0501.2005.01108.x
21. OSSIX PLUS—GLYMATRIX™ Technology in Brief, (n.d.)
22. OSSIX ® PLUS Instructions for Use IFU-MKT-OSP-016 ver OSSIX ® PLUS The Resorbable Collagen Membrane Instructions for Use for OSSIX ® PLUS, (2016)
23. Ghanaati S, Booms P, Orlowska A, Kubesch A, Lorenz J, Rutkowski J, Landes C, Sader R, Kirkpatrick C, Choukroun J (2014) Advanced platelet-rich fibrin: a new concept for cell-based tissue engineering by means of inflammatory cells. J Oral Implantol 40(6):679–689. https://doi.org/10.1563/aaid-joi-D-14-00138
24. Choukroun J, Ghanaati S (2017) Reduction of relative centrifugation force within injectable platelet-rich-fibrin (PRF) concentrates advances patients' own inflammatory cells, platelets and growth factors: the first introduction to the low speed centrifugation concept. Eur J Trauma Emerg Surg. https://doi.org/10.1007/s00068-017-0767-9
25. Miron RJ, Fujioka-Kobayashi M, Hernandez M, Kandalam U, Zhang Y, Ghanaati S, Choukroun J (2017) Injectable platelet rich fibrin (i-PRF): opportunities in regenerative dentistry? Clin Oral Investig. https://doi.org/10.1007/s00784-017-2063-9
26. Ghanaati S, Kirkpatrick C, Kubesch A, Lorenz J, Sader R, Udeabor S, Barbeck M, Choukroun J (2014) Induction of multinucleated giant cells in response to small sized bovine bone substitute (Bio-Oss TM) results in an enhanced early implantation bed vascularization. Ann Maxillofac Surg 4:150. https://doi.org/10.4103/2231–0746.147106
27. Ghanaati S, Orth C, Unger RE, Barbeck M, Webber MJ, Motta A, Migliaresi C, James Kirkpatrick C (2010) Fine-tuning scaffolds for tissue regeneration: effects of formic acid processing on tissue reaction to silk fibroin. J Tissue Eng Regen Med 4:464–472. https://doi.org/10.1002/term.257
28. Serrano C, García-Fernández L, Fernández-Blázquez JP, Barbeck M, Ghanaati S, Unger R, Kirkpatrick J, Arzt E, Funk L, Turón P, del Campo A (2015) Nanostructured medical sutures with antibacterial properties. Biomaterials 52:291–300. https://doi.org/10.1016/j.biomaterials.2015.02.039
29. Choukroun J, Ghanaati S (2016) Reduction of relative centrifugation force within injectable PRF—(platelet-rich-fibrin) concentrates advances patients' own inflammatory cells, platelets and growth factors: first introduction of the low speed centrifugation concept (LSCC), Eur J Trauma Emerg Surg. accepted
30. MacLauchlan S, Skokos EA, Meznarich N, Zhu DH, Raoof S, Shipley JM, Senior RM, Bornstein P, Kyriakides TR (2009) Macrophage fusion, giant cell formation, and the foreign body response require matrix metalloproteinase 9. J Leukoc Biol 85(4): 617–626. https://doi.org/10.1189/jlb.1008588
31. Anderson JM, Rodriguez A, Chang DT (2008) Foreign body reaction to biomaterials. Semin Immunol 20(2):86–100. https://doi.org/10.1016/j.smim.2007.11.004
32. McNally AK, Anderson JM (2011) Macrophage fusion and multinucleated giant cells of inflammation. Adv Exp Med Biol 713:97–111. https://doi.org/10.1007/978-94-007-0763-4_7
33. McNally AK, Anderson JM (2003) Foreign body-type multinucleated giant cell formation is potently induced by alpha-tocopherol and prevented by the diacylglycerol kinase inhibitor R59022. Am J Pathol 163(3):1147–1156. http://www.ncbi.nlm.nih.gov/pubmed/12937156. Accessed 27 Jan 2017. https://doi.org/10.1016/S0002-9440(10)63474-8
34. Ghanaati S, Barbeck M, Orth C, Willershausen I, Thimm BW, Hoffmann C, Rasic A, Sader RA, Unger RE, Peters F, Kirkpatrick

CJ (2010) Influence of β-tricalcium phosphate granule size and morphology on tissue reaction in vivo. Acta Biomater 6(12): 4476–4487. https://doi.org/10.1016/j.actbio.2010.07.006

35. Lorenz J, Kubesch A, Korzinskas T, Barbeck M, Landes C, Sader RA, Kirkpatrick CJ, Ghanaati S (2015) TRAP-positive multinucleated giant cells are foreign body giant cells rather than osteoclasts: results from a split-mouth study in humans. J Oral Implantol 41(6): e257–e266. https://doi.org/10.1563/AAID-JOI-D-14-00273
36. McNally AK, Anderson JM (2005) Multinucleated giant cell formation exhibits features of phagocytosis with participation of the endoplasmic reticulum. Exp Mol Pathol 79(2):126–135. https://doi.org/10.1016/j.yexmp.2005.06.008
37. Enelow RI, Sullivan GW, Carper HT, Mandell GL (1992) Cytokine-induced human multinucleated giant cells have enhanced candidacidal activity and oxidative capacity compared with macrophages. J Infect Dis 166(3):664–668. https://doi.org/10.1093/infdis/166.3.664
38. Zubery Y, Goldlust A, Alves A, Nir E (2007) Ossification of a novel cross-linked porcine collagen barrier in guided bone regeneration in dogs. J Periodontol 78(1):112–121. https://doi.org/10.1902/jop.2007.060055
39. Gautieri A, Redaelli A, Buehler MJ, Vesentini S (2014) Age- and diabetes-related nonenzymatic crosslinks in collagen fibrils: candidate amino acids involved in advanced glycation end-products. Matrix Biol 34:89–95. https://doi.org/10.1016/j.matbio.2013.09.004
40. Bourne JW, Lippell JM, Torzilli PA (2014) Glycation cross-linking induced mechanical-enzymatic cleavage of microscale tendon fibers. Matrix Biol 34:179–184. https://doi.org/10.1016/j.matbio.2013.11.005
41. Rothamel D, Schwarz F, Sculean A, Herten M, Scherbaum W, Becker J (2004) Biocompatibility of various collagen membranes in cultures of human PDL fibroblasts and human osteoblast-like cells. Clin Oral Implants Res 15(4):443–449. https://doi.org/10.1111/j.1600-0501.2004.01039.x
42. Klinger A, Asad R, Shapira L, Zubery Y (2010) *In vivo* degradation of collagen barrier membranes exposed to the oral cavity. Clin Oral Implants Res 21(8):873–876. https://doi.org/10.1111/j.1600-0501.2010.01921.x
43. Zubery Y, Nir E, Goldlust A (2008) Ossification of a collagen membrane cross-linked by sugar: a human case series. J Periodontol 79(6):1101–1107. https://doi.org/10.1902/jop.2008.070421